Effect of Film Forming Amine on Magnetite Deposition Behaviors of Alloy 690TT Tube in Secondary Water Condition

Yong-Beom Lee[a,b], Do Haeng Hur[a], Jong-Hyeon Lee[b], Soon-Hyeok Jeon[a,*]
[a]*Materials Safety Technology Development Division, Korea Atomic Energy Research Institute, 989-111, Daedeok-daero, Yuseong-gu, Daejeon, 34057, Republic of Korea*
[b]*Department of Materials Science and Engineering, Chungnam National University, 99, Daehak-ro, Yuseong-gu, Daejeon, 34134, Republic of Korea*
[*]*Corresponding author: junsoon@kaeri.re.kr*

1. Introduction

In secondary water of pressurized water reactors (PWRs), corrosion products are formed on the surfaces of carbon steel piping and components and inevitably transported into steam generators (SGs). The corrosion products are deposited on SG tubes, tube sheets, and tube support structures. These deposits are mostly composed of magnetite and can cause several problems, including the reduction of heat transfer, tube support plate clogging, and corrosion acceleration due to the impurity concentration and temperature increase on the surface of SG components [1]. Hence, mitigating the corrosion of SG structural materials has been the primary goal of secondary water chemistry control to enhance the integrity of the PWR secondary system.

A universal strategy to mitigate the magnetite deposits is to control the pH of coolant to minimize the formation of corrosion products in carbon steel or low alloy steel piping [1]. Recently, the addition of film-forming amines (FFAs) with pH control agents such as ethanolamine (ETA), ammonia, and morpholine is widely used to mitigate the corrosion of carbon steel piping [2]. FFAs are known to form nanometer-thick films on the surface of the steels, resulting in a significant reduction of corrosion. Among the many FFAs, octadecylamine (ODA) is commonly applied to protect industrial boilers. ODA produces a uniform film on the steel surface even in the presence of impurities such as chlorides and sulfates [3]. Recently, ODA has been utilized in a nuclear power plant that had not been used for a long time under wet lay-up conditions [4].

As described above, some studies have focused on the effects of FFA addition on the corrosion of structural materials in secondary systems. However, there are only a few studies on the relationship between FFA addition and magnetite deposition behavior, which is an ongoing concern in the PWRs. Therefore, this study was focused on the effect of FFA addition on magnetite deposition behavior on commercial Alloy 690TT tubes.

2. Experimental procedure

2.1 Film formation on SG tube

The tube specimen was used from the commercial Alloy 690TT tube. The chemical composition of the Alloy 690TT tube used in this work is presented in Table 1. The length, inner diameter (ID), outer diameter (OD), and thickness of the tube are 500, 17.00, 19.05, 1.025 mm respectively. One end of the tube was welded with an Alloy 600 cap.

Table I: Chemical composition of Alloy 690TT tube (wt. %).

Cr	Fe	Si	Mn	Ti	Al	C	Ni
29.3	10.4	0.3	0.3	0.3	0.2	0.02	Bal.

Before the operating plant, FFA is generally used to form the organic films in the wet lay-up stage. Hence, films were previously formed in an autoclave and deposition test were performed. The film was formed on surface of the specimens in a static autoclave for 10 days at 230 ºC (Fig. 1). Two types of specimens were inserted into the autoclave; Alloy 690TT tube specimen for magnetite deposition test and some Alloy 690TT plate specimens for film characteristics (zeta potential, wettability and roughness). The film-forming solution was used to the deionized (DI) water containing 25 ppm ETA and 500 ppm of ODA.

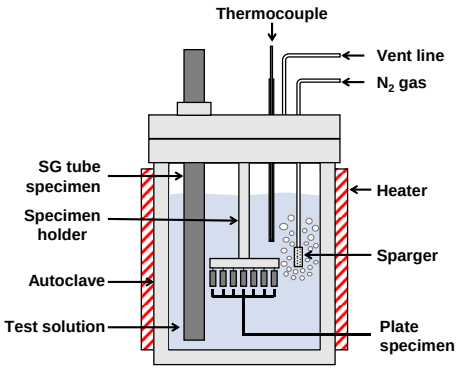

Fig. 1. A schematic diagram of film formation on SG tube and plate specimens.

2.2 Magnetite deposition test

After forming the film on surface of Alloy 690TT tube, the magnetite deposition test was performed in simulated secondary water using a recirculation loop system. Fig. 2 shows a schematic diagram of the magnetite deposition loop system. The pressure in the test section was maintained at 60 bar, which is higher than the saturation pressure at 270 °C. After that, the preheater, band heater, and cartridge heater were heated

sequentially to reach 270 °C. The heat flux was adjusted to about 30 W/cm^2, and the flow rate of the test solution was 260 ml/min.

After the pressure and temperature of the loop system were stabilized, the Fe(II)-acetate solution was continuously injected at 1 ml/min from the bottom of the test section. Fe(II)-acetate is synthesizing simply to pure nanometer-sized particles in water purged with argon gas [5]. The Fe concentration was maintained at about 1 ppm in the test section.

During the test, the dissolved oxygen (DO) level in the loop system was constantly maintained below 5 ppb by purging with nitrogen gas. The test was performed for 14 days.

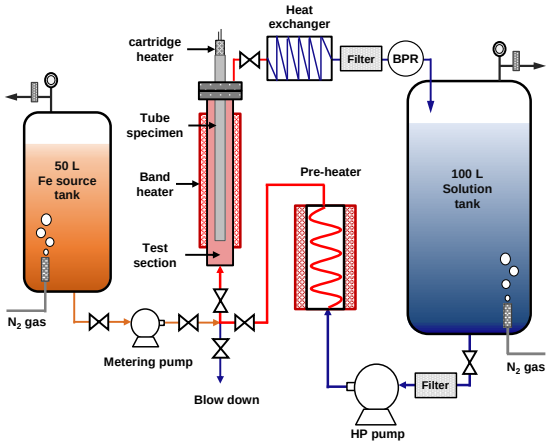

Fig. 2. A schematic diagram of the magnetite deposition loop system.

2.3 Microstructure of film and magnetite deposits

The wettability and surface roughness of film were measured using contact angle and surface profiler. In addition, the chemical species of film was observed using X-ray photoelectron spectroscopy (XPS) analysis. The surface morphology of the film formed on the tube and magnetite deposits was observed using scanning electron microscopy (SEM). Cross-section of the film and deposits was analyzed using a focus ion beam (FIB) technique. The two-dimensional porosity of the deposits was evaluated using an image analyzer. These results will be shown in the oral presentation session.

2.4 The amount of magnetite deposits

The magnetite deposits were selectively dissolved by a chemical cleaning process, and then the dissolved Fe ion concentration in the cleaning solution was measured using inductively coupled plasma atomic emission spectroscopy (ICP-AES) analysis. After that, the measured Fe concentration was converted to the amount of magnetite per unit area. These results also will be shown in the oral presentation session.

3. Results and discussion

3.1 Characterization of the film formed on SG tube

Fig. 3 shows the water droplet images and corresponding static contact angle data. The as-received Alloy 690 plate specimen surface had a contact angle of 77 ± 1°, whereas the film formed plate specimen surface showed a significantly higher value of 110 ± 2°. The contact angle is a measure of the wettability of a surface, i.e., whether the surface was hydrophilic or hydrophobic. Here, a high contact angle corresponds to a lower surface wettability. Therefore, this result indicated that the film-formed surface has a more hydrophobic property than the as-received surface.

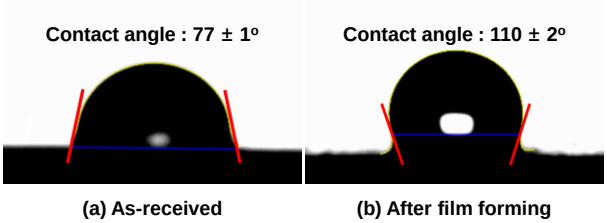

Fig. 3. Static contact angles of water droplets on Alloy 690 plate specimen surfaces: (a) the as-received surface and (b) the film surface formed by addition of ODA.

Fig. 4 shows the surface morphology of the as-received SG tube and film formed on SG tube surface. The outer surface of the as-received SG tube was flat and smooth. The film formed on SG tube surface had a petal-like morphology. The morphology of the film was homogeneous on the whole surface. This result shows that the surface morphology could be greatly affected by the ODA addition.

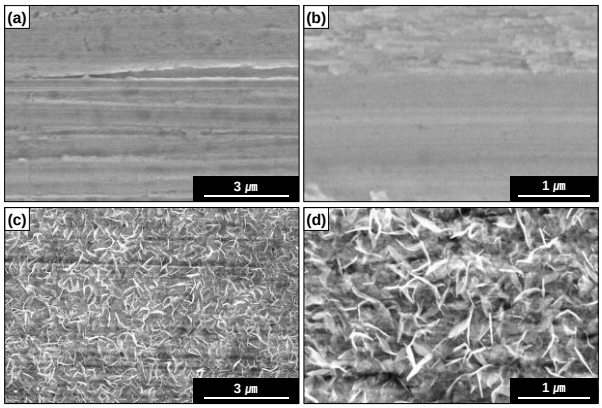

Fig. 4. SEM images of as-received surface and film surface formed by ODA addition: (a), (b) as-received surface and (c), (d) film surface.

Surface roughness was also a very important factor about the hydrophobic respect and deposition behavior. However, the roughness was no significant difference between the as-received surface and film formed on tube surface. The root-mean-square roughness (R_q) of both specimens was almost the same value (about 0.24~0.26 μm).

Fig. 5 shows the chemical composition of the film formed on SG tube using SEM-EDS analysis. The film

was mostly composed of C (about 89.85 at. %), N and O were composed of 5.66 at. % and 3.49 at. %, respectively, and the metallic elements such as Cr, Ni, and Fe were rarely detected.

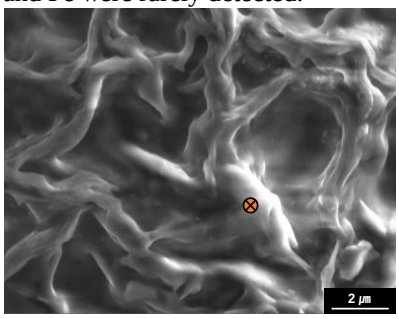

Element	at.%
C K	89.85
N K	5.66
O K	3.49
Cr K	0.58
Fe K	0.09
Ni K	0.33

Fig. 5. SEM-EDS analysis of film formed on SG tube by addition of ODA.

Fig. 6 shows the XPS survey spectra of film formed on SG tube by ODA addition. The peaks of C, O, and N elements were prominently observed, and the peaks of metal elements of Cr, Ni, and Fe were extremely small. This result was well consistent with the SEM-EDS result.

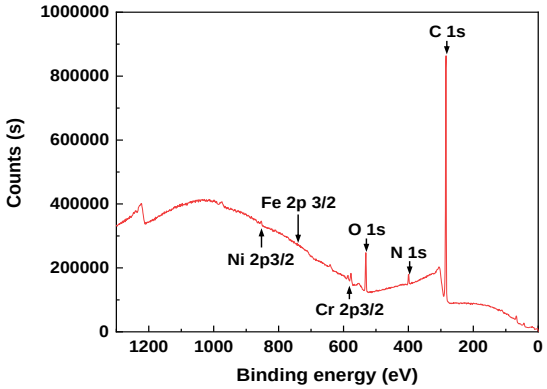

Fig. 6. XPS spectra of the film formed on SG tube by addition of ODA.

Fig. 7 shows the high-resolution XPS spectra from the specimen filmed with ODA. Table 3 summarizes the binding energy, full width half maximum (FWHM) of components, and the fraction of components (at. %) of the film calculated by integration of peak area for each component. The C 1s spectrum had three peaks: the first one at 285.0 EV could be ascribed to the aliphatic C-C bonds of the ODA molecule [6]. The second one at 286.1 eV was attributed to C-N bond. The third one at 288.3 eV was ascribed to O=C-O bond. The N 1s spectrum exhibits two peaks at 399.5 eV and 401.1 eV which could be assigned to the NH_2 and NH_3^+ components. The O 1s spectrum was consisted of three peaks: a first one at 530.0 eV related to O_2, and a second one at 531.5 was attributed to the C-O bond, a third one at 532.5 eV was attributed to the OH^- ions. For the Fe 2p3/2 spectrum, a first peak appears at 707.9 eV due to metallic Fe and a second peak at 711.8 eV related to Fe oxide. The Cr and Ni 2p3/2 spectrums were also displayed the metallic Cr and Ni and oxide or hydroxide components.

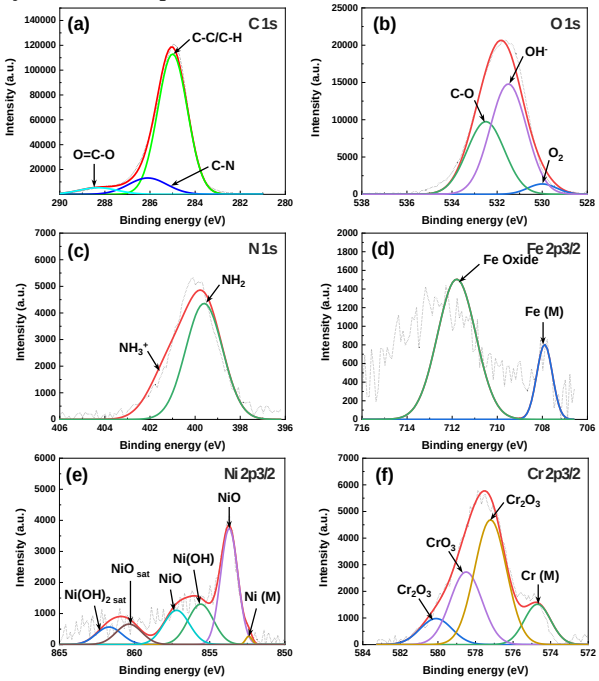

Fig. 7. High-resolution XPS spectra of the film formed on SG tube by addition of ODA: (a) C 1s, (b) O 1s, (c) N 1s, (d) Fe 2p3/2, (e) Ni 2p3/2, (f) Cr 2p3/2

Table 2. The binding energy and FWHM of compounds for each elements and total fraction of components obtained from high-resolution XPS spectra.

Components		Binding energy (eV)	FWHM (eV)	at. %
C	C-C, C-H	285.0	1.5	56.56
	C-N	286.1	2.0	8.53
	O=C-O	288.3	2.0	3.45
O	O_2	530.0	1.5	0.67
	C-O	531.5	1.9	6.16
	OH^-	532.5	1.9	9.11
N	NH_2	399.5	1.9	2.72
	NH_3^+	401.1	2.0	1.32
Cr	Cr (M)	574.7	1.3	0.82
	Cr_2O_3	577.2	2.0	3.03
	CrO_3	578.5	2.0	1.77
	CrO_3	580.1	2.0	0.63
Fe	Fe (M)	707.9	0.8	0.21
	Fe oxide	711.8	2.0	0.98
Ni	Ni (M)	852.4	0.5	0.04
	NiO	853.7	1.4	1.63
	$Ni(OH)_2$	855.6	2.0	0.85
	NiO	857.2	2.0	0.72
	NiO sat	860.4	2.0	0.43
	$Ni(OH)_2$ sat	861.7	2.0	0.37

3.2 Characteristics and amount of magnetite deposits

Fig. 8 presents the surface morphologies of magnetite deposits on the as-received tube. Various sized particles within the range of about 100 nm to 2 μm were observed and had polyhedral or spherical shapes. In addition, a number of pores between the particles was also observed.

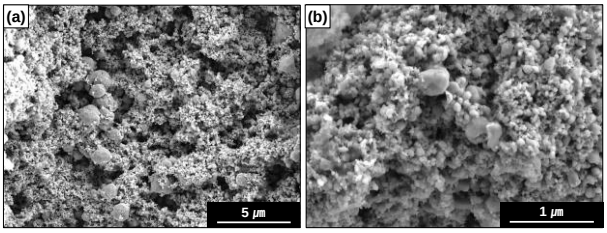

Fig. 8. SEM images of surface morphologies of as-received SG tube: (a) low magnification and (b) high magnification.

Fig. 9 shows the cross-sectional SEM images of the deposits in as-received SG tube. Numerous micro-pores were clearly observed in the deposits. The pores form when steam bubbles escape from a heated specimen surface and serve as a site for the accumulation of various chemical impurities. The chemical impurities concentrated in the pores could adversely affect the SG integrity [7].

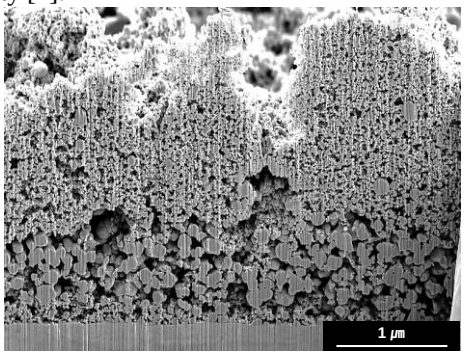

Fig. 9. Cross-sectional SEM images of magnetite deposits in non-filmed specimen.

The magnetite deposition test of the film formed on SG tube is currently in progress. The morphology and the amount of magnetite accumulated on film will be presented in oral session. In addition, mechanism of ODA addition on the magnetite deposition behavior will be discussed.

4. Conclusions

(1) The film formed on SG tube surface had a petal-like morphology. The film was mostly composed of C, N, and O and a small amount of metallic elements such as Cr, Ni, and Fe were observed. In addition, the film formed surface had a more hydrophobic property than the as-received surface.

(2) The hydrophobic film characteristics and zeta potential could affect the magnetite deposition behavior on SG tube. The zeta potential measurement and magnetite deposition test of the film formed on SG tube is currently in progress. These results will be shown in the oral presentation session.

ACKNOWLEDGEMENTS

This work was supported by the National Research Foundation (NRF) grant of the Republic of Korea funded by the Korean government (NRF-2017M2A8A4015159).

REFERENCES

[1] C. Marks, Steam Generator Management Program: Effects of different pH control agents on pressurized water reactor plant systems and components, EPRI, Palo Alto, CA, USA (EPRI report 1019042), 2009.
[2] A.V. Ryzhenkov, S.I. Pogorelov, A.V. Kurshakov. Prospects for the application of film-forming amines in power engineering, Contact Surf., 127-137. 2015
[3] H.-H. Ge, G.-D. Zhou, Q.-Q. Liao, Y.G. LEE, and B.H. LOO. A study of anti-corrosion behavior of octadecylamine-treated iron samples, Appl. Surf. Sci., 156, p 39-46. 2000
[4] S. Odar. Use of film forming amines (FFA) in nuclear power plants for lay-up and power operation, A.N.T. International., 2017.
[5] R. Vijayakumar, Y. Koltypin, I. Felner, A. Gedanken, Sonochemical synthesis and characterization of pure nanometer-sized Fe3O4 particles. Mater. Sci. Eng. A. 286, 101-105. 2000
[6] N. Alzate-Carvajal, E.V. Basiuk, V. Meza-Laguna, I. Puente-Lee, M.H. Farías, N. Bogdanchikova, V.A. Basiuk, Solvent-free one-step covalent functionalization of graphene oxide and nano-diamond with amines, RSC Adv. 6 113596-113610. 2016
[7] P.J. Millet, J.M. Fenton, A detailed model of localized concentration processes in porous deposits of SGs. In Proceedings of the 5th International Symposium on Environmental Degradation of Materials in Nuclear Power Systems-Water Reactors, Monterey, CA, USA, pp. 745-751, 1991.